SCIENCE CHINA
Technological Sciences

•Article•

July 2018 Vol.61 No.7: 949–958
https://doi.org/10.1007/s11431-017-9202-y

Formation of wavy-ring crack in drying droplet of protein solutions

GAO MengNi[1,2], HUANG XianFu[1,2] & ZHAO YaPu[1,2*]

[1] *State Key Laboratory of Nonlinear Mechanics, Institute of Mechanics, Chinese Academy of Sciences, Beijing 100190, China;*
[2] *School of Engineering Science, University of Chinese Academy of Sciences, Beijing 100049, China*

Received September 14, 2017; accepted January 18, 2018; published online May 17, 2018

The formations of desiccation cracks and their patterns in drying droplets of protein solutions are studied experimentally. The solvent evaporation causes the dehydration self-organization phenomenon in colloidal droplets, followed by the formations of desiccation cracks. Two categories of highly ordered crack patterns, which we name "daisy" and "wavy-ring", are identified in the drying droplets. We explore the shifting of crack patterns from the "daisy" to the "wavy-ring" by varying the concentration of protein droplets. The results show that the concentration correlates with the pattern of deposition film directly, and modulates the periodicity of the crack pattern. We investigate the formations and periodicities of these two kinds of crack patterns, and obtain the scaling law of periodicity of the "wavy-ring" crack pattern. The relationship between the deposition pattern and the highly ordered crack patterns is also examined. This study will help in understanding the formation mechanisms of crack patterns in drying droplets of protein solutions and assist the future design of crack patterns in practical applications.

coffee-ring effect, spiral crack, self-organization, crack pattern, desiccation

Citation: Gao M N, Huang X F, Zhao Y P. Formation of wavy-ring crack in drying droplet of protein solutions. Sci China Tech Sci, 2018, 61: 949–958, https://doi.org/10.1007/s11431-017-9202-y

1 Introduction

Desiccation crack is a general phenomenon in nature and has aroused scientists' attention for centuries. As early as 1917, Kindle [1] studied on mud crack experimentally in the lab and obtained different mud crack patterns by varying the components of mud and the velocity of the desiccation. Drying is one of the most often used methods in thin film preparation [2]. However, along with the drying process, cracks may originate and propagate. Fascinating crack structures and patterns formed by desiccation have been observed in different types of hard film/soft substrate systems [3,4]. In recent years, there has been an increasing number of reports on crack morphologies and final patterns in thin films, such as spiral cracks [5,6], oscillating cracks [7–9], annular cracks [10,11], etc. Kattouf et al. [12] proposed a corresponding model of the nucleation and development to study the generation of perfect periodically hexagonal crack patterns. These attractive desiccation crack patterns have been found useful in traditional art field and industry. Craquelure patterns can help identify the age of oil paintings [13–15]. Preventing the troublesome cracks and developing the crack patterns in practical applications are of more interest, such as the fabrication of nanoelectronic and microfluidic devices [16,17] and industrial applications in printing [18–20].

To utilize desiccation cracks in thin film preparation, understanding the underlying mechanisms of crack pattern formation is of great significance. Experimental and theoretical efforts have been infused into the studies of the formation of these crack patterns. The cracking dynamics and pattern transitions in some colloidal droplets were studied [21–23]. Pauchard et al. [24] obtained both regular and disordered patterns in colloidal suspension depending on the

* Corresponding author (email: yzhao@imech.ac.cn)

suspension salinity. Leung et al. [25] and Néda et al. [26] focused on spiral cracks in thin films of drying suspension of precipitate and proposed a mesoscopic spring-block model to simulate this desiccation spiral crack. Wu et al. [27] studied Archimedes spiral cracks in a nanofilm. The conditions that influence the formations of crack patterns were also explored, such as the desiccation direction (by controlling temperature and humidity) [28–31], an electric field [32,33], and a magnetic field [34].

It also has long been known that drying droplets of biological solutions may crack due to the evaporation of the solvent, such as DNA [35], human blood [36,37], human tears [38], protein solutions [39,40], etc. Brutin et al. [36] reported that the patterns formed in droplets of human blood can be used to tell whether persons are in good health. A blood drop of a healthy person will generate regular and ordered crack pattern, in contrast to messy cracks formed in that of a person with hyperlipidaemia or anaemia. Sobac and Brutin [37] also found that the wettability influences the final pattern of a drying blood droplet. Studies on crack patterns of drying droplets of human tears pointed out that these patterns can be used to diagnose eye disease in patients [38]. Golbraikh et al. [40] revealed that crack patterns were phenomenologically the same as an array of cracks and provided a model to describe the formation of this crack pattern from the view of crystallization. However, owing to the complex composition of biological fluids and multi-physical-chemical-mechanical processes, the mechanisms of different crack patterns caused by spontaneous evaporation still stay unexplained. Because of the diversity of cracks, it is difficult to explain the whole details of pattern formation by analytical formulations or a single model.

In this paper, we study the formations of typical patterns in drying droplets experimentally using a protein solution (i.e., aqueous egg-white solutions for representation). Various cracks form quite different patterns in the droplets with different concentrations. We investigate the influence of complete drying process on the final pattern and classify these patterns. Then the formation mechanisms of these crack patterns and their peculiar periodicities are further explored.

2 Materials and methods

To study multifarious cracks and their patterns in drying droplets, we selected a protein solution, i.e., egg-white solution—A typical and common biological fluid, to perform the experiments. The raw egg-white solution is formed primarily by 10% proteins (approximately 148 kinds of proteins and ovalbumin is the most abundant one) dissolved into 90% water. Deionized water was used to dilute the raw egg-white solution. We varied the dilution multiple α with 0, 0.2, 1, 10, 25, 50, 90, 100, 125, 150, 170, 200, 300, 400 and 500 for experimental samples. As a result, the volume concentration of proteins c changed from 10% to 0.19‰, as listed in Table 1.

The experiments were conducted on a vibration-damping platform. Protein droplets of different concentrations with a volume of 2 μL were deposited on the surface of clean silicon wafer Si (100) using a micropipette. Then the droplets evaporated under room temperature (25°C) and ambient pressure (1 atm) with a relative humidity (RH) ~20%. The drying processes were captured using a three-dimensional digital microscope (HIROX KH8700 with MX-mount lens of 5040RZ and 10C) right above the droplets at a frame rate of 24 fps. At the same time, a contact angle meter (Dataphysics OCA-20) was used to observe lateral profiles of the droplets in real-time at a frame rate of 0.5 fps. At last, a contact surface profiler (Bruker DektakXT with contact radius r_c=2.5 μm and contact force f_c=1 mN) was employed to measure three-dimensional profiles of the deposition films. The experiments were repeated more than dozens of times.

3 Results and discussion

3.1 Droplet evaporation process

When the droplet was dripped on the surface, the evaporation of solvent started. To explore the evaporation process, we measured the dynamic evolution of contact angles of droplet during the evaporation process. The time required for the whole evaporation was about 5–10 min, which depended on the concentration and the volume of the droplet. Figure 1 presents the evolution of contact angles of the drying droplets with the concentrations 83.33‰ and 0.50‰. As the protein droplets dried, particles (proteins) assembled at the

Table 1 The concentration of proteins (c) in the aqueous egg-white solutions versus the dilution multiple (α)

Dilution multiple (α)	Concentration of proteins (c)
0.2	83.33‰
1	50.00‰
10	9.09‰
25	3.85‰
50	1.96‰
90	1.09‰
100	0.99‰
125	0.79‰
150	0.66‰
170	0.58‰
200	0.50‰
300	0.33‰
400	0.25‰
500	0.19‰

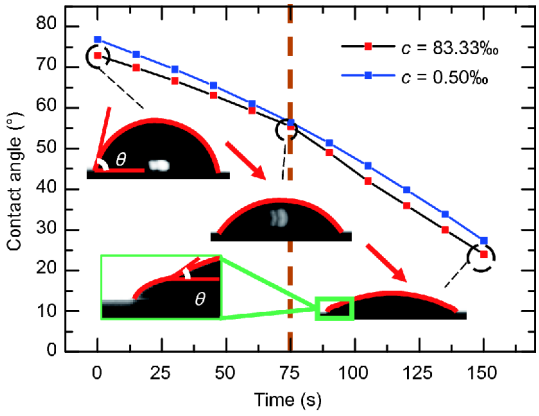

Figure 1 (Color online) The evolution of contact angles of droplets with the protein concentrations 83.33‰ and 0.50‰. Compared with continuous change of the droplet with a low concentration, a shift point indicates that a gelled foot develops at the edge of the droplet with a high concentration. Insets: corresponding profiles of the droplet with the concentration 83.33‰.

three-phase contact line [41,42]. Since the particles pinned the contact line onto the substrate, droplets dried under constant area condition. Therefore, the contact angles decreased with the evaporation process proceeding.

At first, the contact angles of these two kinds of droplets (concentrations 83.33‰ and 0.50‰) changed smoothly with little difference. As the evaporation was continuing, the main difference emerged. For the protein droplets with concentration 0.50‰, the contact angles changed continuously, however, those of the protein droplets with concentration 83.33‰ experienced a shift point. The particles accumulated at the interphase boundary and finally aggregated to form a gelled film when the particles got more concentrated, while the central part of the droplets remained liquid [24]. Supporting material Movie 1 exhibits the dynamic drying processes of droplets with different concentrations.

During the drying process, the relative motion of particles to the solvent causes Stokes drag force acting on particle surfaces. Assuming the protein molecules as equal spheres, we can calculate the Stokes force

$$F_{\text{drag}} = 3\pi\mu D u, \tag{1}$$

where μ is the dynamic viscosity, D is the average hydrodynamic diameter of a protein and u is the flow velocity. Taking no account of the interactions of particles, the effective viscosity of the dilute solution increases with the volume concentration of the solute as $\mu_{\text{eff}} \approx \mu(1+5c/2)$ [43]. Hence, a relatively high concentration will generate a high effective viscosity. As the particles get more and more concentrated, they eventually touch each other. Thus the maximum capillary force between two adjacent particles is expressed as [44]

$$F_{c,\max} = -\frac{2\pi D\gamma\cos\theta_1}{3}, \tag{2}$$

where γ is the solvent-air interfacial tension and θ_1 is the contact angle between the solvent and particle. The evaporation of solvent drives the self-organization of particles in the drying protein droplets and finally forms a thin film on the substrate. Understanding the drying and deposition processes is the first step to investigate the formations of desiccation cracks.

3.2 Deposition films and their patterns

At the end of droplet evaporation, the droplets solidified and finally formed annular or circular thin films. As shown in Figure 2, there were four typical deposition patterns observed in our experiments by varying the concentration (negatively correlated with the dilution multiples) of the protein solutions. The lower the concentration became, the more obvious the coffee-ring effect was. This is ascribed to the competition among different flows in the droplets. Figure 3(a) displays three flows [45], namely the radial flow, the Marangoni recirculating flow and the vertical flow. The first flow, whose magnitude depends on the ratio of evaporative mass flux and the density of droplets [46], tends to form an annular deposition pattern. The second flow resulting from the surface tension gradient [47] leads to a mountain shape. While the last flow gives rise to a flat film. Driven by Derjaguin-Landau-Verwey-Overbeek (DLVO) interactions, the particles move toward the substrate [48]. The velocity of this flow is estimated as $V_{\text{D}} \sim 2F_{\text{D}}/6\pi\mu D$, where F_{D} is the DLVO force that is a long-range interaction and refers to the algebraic sum of van der Waals and the electrostatic forces [49]. Shape of the droplet changes during the evaporation as illustrated in the schematic of droplet profiles in Figure 3(b). In our experiments, all deposition films had coffee ring, however, the thickness of the film and the width of the coffee ring were quite different. According to Figure 3(c), to quantitatively examine the relationship between the deposition pattern and the concentration, we chose two dimensionless parameters to depict the deposition pattern, i.e., $\chi_L = L / R_0$ that refers to the coffee-ring width normalized by the initial droplet radius and $\chi_H = H_c / H_{\max}$ that is the central thickness normalized by the maximum thickness $H_{\max}$. Figure 3(d) reveals that both χ_L and χ_H increase with the solution concentration.

3.3 Desiccation cracks and their patterns

As the deposition process finished and the drying was going on, desiccation cracks originated in the drying film. A fully desiccated droplet consisted clearly of two parts, i.e., the coffee ring and the central part. In these two parts, we discovered quite distinct desiccation cracks and a few highly ordered crack patterns (see Figure 4). These typical

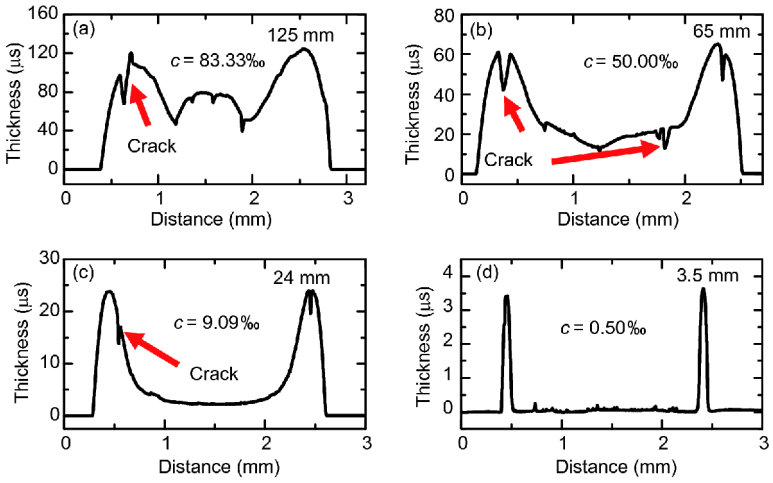

Figure 2 (Color online) Four typical deposition patterns of drying protein droplets. The gaps indicate cracks on the film surface. Their radii are almost equal, while their shape and thicknesses are quite distinct with the maximum thickness about 3–130 μm, (a) c=83.33‰, a center bump, (b) c=50.00‰, a slope in the central part, (c) c=9.09‰, a coffee ring, (d) c=0.50‰, a coffee ring with the center thickness about zero.

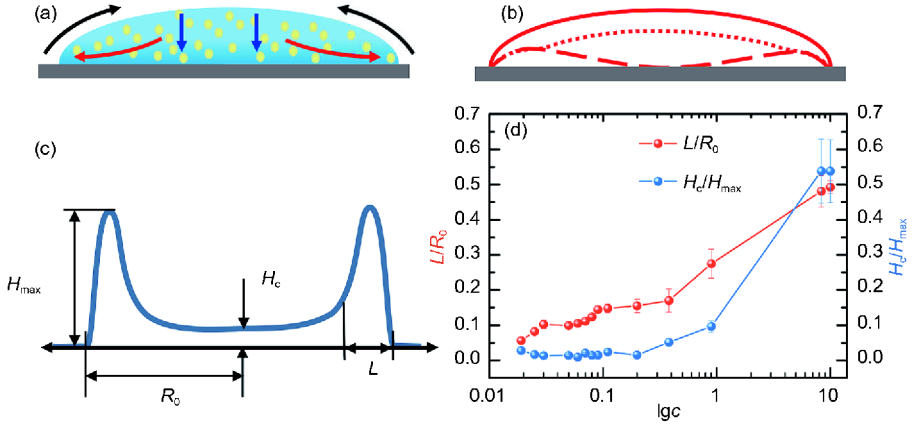

Figure 3 (Color online) (a) Schematic of three flows. The competition of these flows in the droplet leads to the final deposition pattern. (b) As the evaporation proceeds, profile of a drying droplet changes. (c) A fully desiccated droplet consists of two regions. Four geometric parameters can describe the film: H_{max} and L are the thickness and the width of the coffee ring, H_c is the thickness of the central part and R_0 is the radius. (d) The dimensionless width of the coffee ring $\chi_L=L/R_0$ and the dimensionless thickness $\chi_H=H_c/H_{max}$ are chosen to depict the film. Both of them increase with the concentration.

morphologies of crack patterns are divided into two broad categories, according to whether their cracks propagated into the central part of the film or not, which we name "daisy" (Figure 4(a) and (b)) and "wavy-ring" (Figure 4(c) and (d)). The Figure 4(e) is a high-definition picture of a "wavy-ring" crack pattern. In this section, we display the details and formations of these two patterns.

3.3.1 The "daisy" pattern

The "daisy" pattern is mainly formed by uniformly arranged radial cracks that originate at the periphery and propagate towards the center. This category of pattern appeared when the concentration of droplets exceeded ~9‰ that was relatively high. It was also observed in other drying colloidal solutions with high concentrations [24]. Besides the radial cracks, curved cracks, spiral cracks, and chaotic cracks were also observed in one drying protein droplet in our experiments, as detailed in Figure 5(a). Curved cracks originated at the perimeter of the drying droplet (Figure 5(b)), and then propagated into the center of the dried protein film radially (Figure 5(c)). When these radial cracks were inclined to stop, they would deflect at the center where cracks were chaotic (Figure 5(d)). In addition, during the drying process, tensile stress generates in the film [50]. Here the residual stress has gradient distribution through the thickness of the film. This stress is maximum at the film/substrate interface and vanishes at the free surface of the film. As a result, cracks generate at the bottom, and then propagate to the surface of the film. More details of the chaotic cracks in our experiments are visible in Figure 5(e), where obscure cracks under the film surface are also demonstrated. Movie 2 presents the formation of the "daisy" pattern.

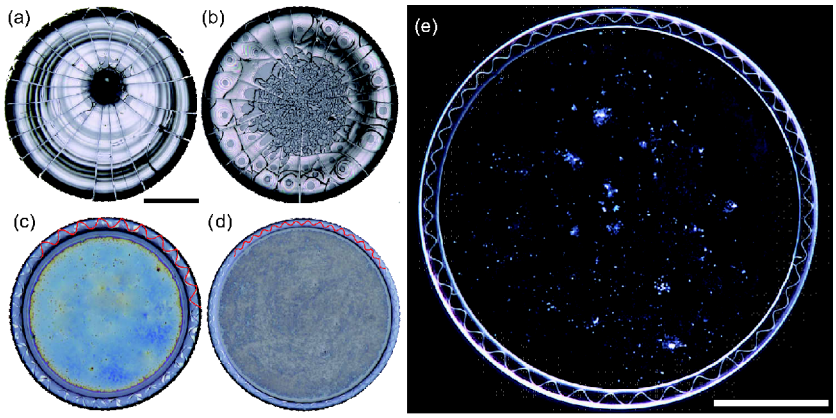

Figure 4 (Color online) Typical crack patterns and their categories. (a), (b) The "daisy" pattern: regularly arranged cracks initiate at the edge and propagate radially to the center of drying droplets. (c), (d) The "wavy-ring" pattern: template self-replicates inside the coffee ring. (c) A saw-toothed template; (d) a sinusoidal template; (e) a high-definition picture of a "wavy-ring" pattern. The scale bars represent 1 mm.

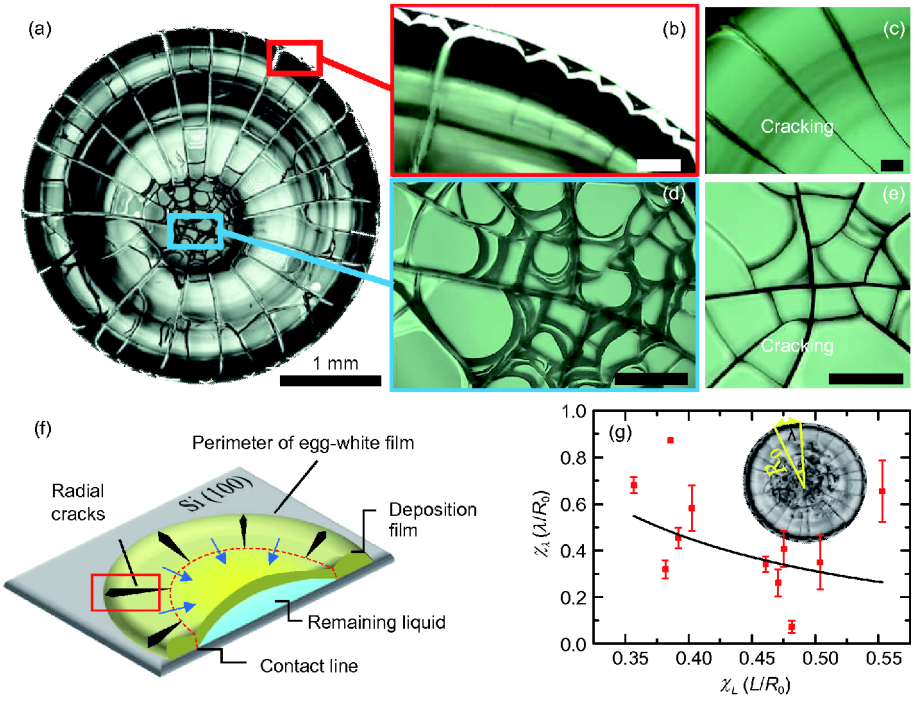

Figure 5 (Color online) (a) The "daisy" pattern, (b) curved cracks at the edge, (c) radial cracks propagating into the center film, (d) chaotic cracks in the central part, (e) chaotic cracks growing from the bottom to surface of the film. (f) A humidity gradient induces crack propagation in drying droplets. (g) The crack spacing versus the dimensionless width of the coffee ring is measured. The scale bar in (a) represents 1 mm and the scale bars in (b-e) represent 100 μm.

As discussed previously, for a drying droplet with relatively high concentration, a gelled film develops at the triple contact line; by contrast, the central part is still in liquid state during the drying process. Consequently, a humidity gradient generates along the radial direction. These two parts are set apart by a compact front that moves towards the center point continuously. Following the moving front, radial cracks initiate at the edge of the droplet and grow, as shown in Figure 5(f).

We assume that the drying film is under the in-plane stress σ^d, which is caused by the evaporation and proportional to the capillary pressure. To calculate the strain energy release rate G, we need to look at how a single crack releases the stress. Here we define a coordinate system Oxyz located at the crack tip. The thickness direction is defined as the z axis. A crack propagates along the direction of the positive x axis. The stresses released by the crack decay along the normal direction to the crack surface, i.e., the y axis [51]

$$\frac{\mathrm{d}\Delta\sigma_n^d}{\mathrm{d}y} = -\frac{\Delta\sigma_n^d}{l}, \tag{3}$$

where $\Delta\sigma_n^d$ is normal to the crack, y is the normal distance to the crack surface, and l denotes the characteristic decay

length of the stress. Within the decay length, the stress is significant. Here $l=h/\beta$, β is a coefficient related to the mismatch between the substrate and the film and h is a uniform thickness of the film. In our experiments, the substrate is rigid compared with the film. Thus, in the case of uniform thickness, β is about 0.8 [51]. Rearranging eq. (3), we have

$$\frac{\mathrm{d}\Delta\sigma_n^d}{\Delta\sigma_n^d}=-\frac{\mathrm{d}y}{l}, \tag{4}$$

and therefore the general solution of above differential equation is

$$\ln\Delta\sigma_n^d=-\frac{y}{l}+C, \tag{5}$$

where C is the integration constant. The in-plane stress vanishes on the crack surface $y=0$, where it requires $\Delta\sigma_n^d=\sigma^d$. Using this boundary condition, we can obtain the integration constant $C=\ln\sigma^d$. Thus, the released stress yields

$$\ln\frac{\Delta\sigma_n^d}{\sigma^d}=-\frac{y}{l}, \tag{6}$$

and an exponentially decaying stress distribution is

$$\Delta\sigma_n^d(y)=\sigma^d\mathrm{e}^{-|y|/l}. \tag{7}$$

The stress along the direction parallel to the crack is also released by the Poisson effect. Using the Hooke's law, we can find

$$\Delta\sigma_p^d(y)=\nu\Delta\sigma_n^d(y)=\nu\sigma^d\mathrm{e}^{-|y|/l}, \tag{8}$$

where ν is the Poisson's ratio of the film. Hence, the in-plane stresses normal and parallel to the crack are [52]

$$\sigma_n^d=\sigma^d-\Delta\sigma_n^d(y)=\sigma^d(1-\mathrm{e}^{-|y|/l}), \tag{9}$$

$$\sigma_p^d=\sigma^d-\Delta\sigma_p^d(y)=\sigma^d(1-\nu\mathrm{e}^{-|y|/l}). \tag{10}$$

Near a crack tip, the variation of opening stress distributions can be described by K_{I}, and that of shearing stress distributions can be described by K_{II}. They are the stress intensity factors of mode I and mode II, respectively, and related with the energy release rate as $G=\left(K_{\mathrm{I}}^2+K_{\mathrm{II}}^2\right)/E'$, where $E'=E/(1-\nu^2)$ is the plane strain elastic modulus of the film and E is the Young's modulus of the film. It is difficult to calculate the energy release rate G directly. Comparing the strain energy densities before and after cracking, one can finally find that the energy release rate is [51]

$$G=\frac{\left(\sigma^d\right)^2h}{\beta E'}=\frac{\left(\sigma^d\right)^2l}{E'}, \tag{11}$$

where the length scale is the film thickness, not the crack length [53]. As drying continues, the stress σ^d increases. Then for the problem of crack propagation, the Griffith's criterion is employed [54]. When the condition $G=G_{\mathrm{c}}$ is satisfied, the crack grows. Here G_{c} is a material parameter and denotes the critical energy release rate.

For the "daisy" pattern of an array of cracks, the average crack spacing along with the perimeter of the drying droplet λ is discussed. For an array of cracks, the energy release rate G per crack of the array is [55]

$$G=l\frac{\left(\sigma^d\right)^2}{E'}\tanh\frac{\lambda}{2l}. \tag{12}$$

For a brittle case, the wavelength λ is proportional to the film thickness [56]. A possible explanation is that the flow of solvent away from a crack determines the crack spacing [57]. In our experiments, the dimensionless period $\chi_\lambda=\lambda/R_0$ normalized by the radius of the droplet R_0 was measured. The relationship between the dimensionless period and the dimensionless width of the coffee ring is shown in Figure 5(g), which indicates that χ_λ is not proportional to the width. On the contrary, a smaller spacing turns up when the width increases. Actually, the effects of the delamination and the plastic effects of the film make a difference to the spacing.

Moreover, as the deposition film dried further, the film was split into separated blocks in which spiral cracks were discovered. The blocks peeled off from the substrate, as a result, spiral cracks initiated at the edge of the blocks [25]. The colorful interference fringes indicated the peeling of the film (Figure 6(a)). The spiral cracks were triggered from the block edges and by defects, as shown in Figure 6(b). In addition to these single-spiral cracks, double-spiral cracks were observed in some blocks. They always rotated in the same direction in one block, as shown in Figure 6(c). Movie 3 gives the dynamic process of a spiral crack in the central part.

3.3.2 *The "wavy-ring" pattern*

The second category of crack pattern, i.e., the "wavy-ring" pattern, was acquired in drying droplets with low concentrations in our experiments. The critical concentrate was about 10‰–50‰. It is of great interest for its unique position and highly ordered shape. The periodically wavy cracks in the coffee ring render the "wavy-ring" pattern. In this category of crack pattern, there were two kinds of repeating templates of periodic cracks. One was saw-toothed, and the other was sinusoidal. The propagation process of a saw-toothed crack was observed in real time, as shown in Figure 7 (see Movie 4 for the dynamic propagation process). For a droplet with low concentration, the coffee ring took shape at first, followed by the formation of the central part in a few seconds with the droplets evaporating continuously. Then the cracks were triggered by defects where the stress concentrated, and propagated circularly in the coffee ring.

Compared with the growth of radial cracks under the humidity gradient of the whole film, the wavy-ring cracks take final shape in the coffee ring between two boundaries that fix the coffee ring to the substrate, as shown in Figure 8(a). For the coffee ring, the radius of the film is much larger com-

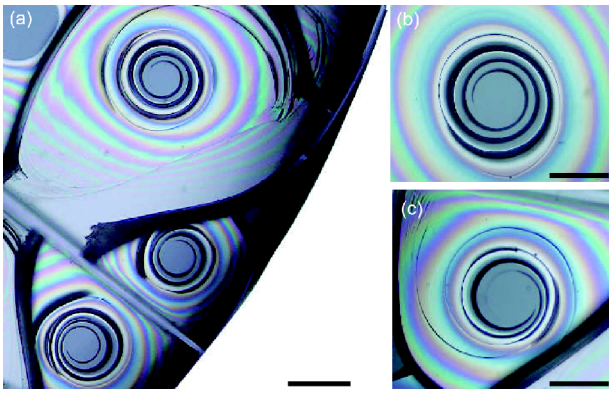

Figure 6 (Color online) (a) Adjacent spiral cracks in blocks, (b) a spiral crack triggered by a defect, (c) a double-spiral crack rotating in one direction. The colorful interference fringes indicate the peeling of the film. All scale bars represent 100 μm.

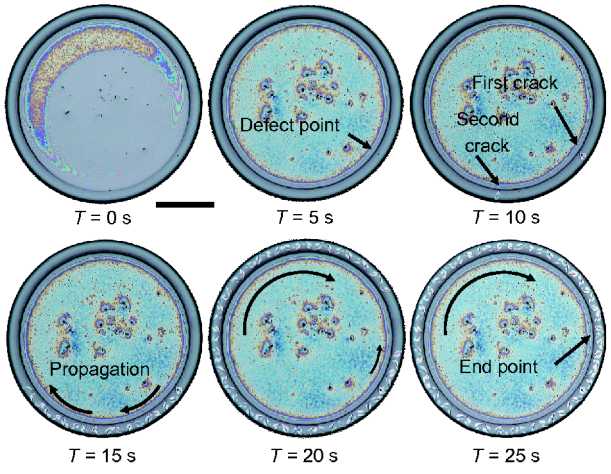

Figure 7 (Color online) Real-time observation of the "wavy-ring" pattern formation. Crack originates from a defect point with a straight one (the radial direction). That a saw-toothed crack self-replicates in the coffee ring forms the pattern. Cracks are perpendicular to each other at the end. The scale bar represents 1 mm.

pared with the width of the coffee ring, so the curvature effect can be neglected. We assume that the coffee ring is a rectangular film under in-plan stress σ^w, as shown in Figure 8 (b). Thus, the outer and inner boundaries are set at $y=\pm L/2$, and the thickness has

$$h = h_0\cos\frac{\pi y}{L},\ \left(-\frac{L}{2}\le y\le\frac{L}{2}\right), \tag{13}$$

with h_0 the thickness of the centerline of the coffee ring and L the width of the coffee ring. The varying thickness affects average in-plane stress, which finally determines the decay length of the stress. We take the two boundaries as two individual straight cracks to calculate the stress distribution in the coffee ring, and assume a uniform thickness $\bar{h}$ and the decay length $\bar{l}$. From eqs. (3)–(5), we find the released stresses of the outer and inner boundaries as

$$\ln\Delta\sigma_{\mathrm{O}}^{w} = -\frac{L/2-y}{\bar{l}} + C_1,\ \left(-\frac{L}{2}\le y\le\frac{L}{2}\right), \tag{14}$$

$$\ln\Delta\sigma_{\mathrm{I}}^{w} = -\frac{y+L/2}{\bar{l}} + C_2,\ \left(-\frac{L}{2}\le y\le\frac{L}{2}\right), \tag{15}$$

where C_1 and C_2 are the integration constants. Then the completely released stress by these two boundaries in the film is

$$\Delta\sigma_n^{w} = \Delta\sigma_{\mathrm{O}}^{w} + \Delta\sigma_{\mathrm{I}}^{w}. \tag{16}$$

Considering the boundary conditions, $\Delta\sigma_n^{w}\big|_{y\pm L/2} = \sigma^w$ and $\Delta\sigma_{\mathrm{O}}^{w}\big|_{y=0} = \sigma_{\mathrm{I}}^{w}\big|_{y=0}$, we obtain the integration constants as

$$C_1 = C_2 = \ln\frac{\sigma^w}{1+\mathrm{e}^{-L/\bar{l}}}, \tag{17}$$

and the released stress as [58]

$$\Delta\sigma_n^{w} = \sigma^w\frac{\mathrm{e}^{y/\bar{l}}+\mathrm{e}^{-y/\bar{l}}}{\mathrm{e}^{L/2\bar{l}}+\mathrm{e}^{-L/2\bar{l}}} = \sigma^w\frac{\cosh\left(y/\bar{l}\right)}{\cosh\left(L/2\bar{l}\right)}. \tag{18}$$

Therefore, the stresses normal and parallel to the crack surface at the distance y are

$$\sigma_n^{w} = \sigma^w - \Delta\sigma_n^{w},\ \sigma_p^{w} = \sigma^w - \nu\Delta\sigma_n^{w}. \tag{19}$$

Using the stress distributions, we calculate the energy release rate of this crack as

$$G = \frac{\bar{h}}{\beta E'}\left[\left(\sigma_n^{w}\cos\varphi\right)^2 + \left(\sigma_p^{w}\sin\varphi\right)^2\right], \tag{20}$$

where φ denotes the angle to the x-axis and the weight function method is applied [59,60]. To achieve the maximum energy release rate, cracks in the coffee ring get wavy due to the oscillations of the stresses from the boundaries to the centerline. In the vicinity of boundaries, the stress components are primarily parallel to the bounding lines. Therefore, the middle crack curves to one side if it grows towards the boundaries. The film near the boundaries is thinner and stiffer, as a result, the location of maximum energy release rate will be at ±90° near the two boundaries. Thus, the crack deflects back to the centerline. Repetition of this process results in the "wavy-ring" pattern.

In a polar coordinate system (r, ψ) with the origin at the center of the film, a sinusoidal-circular crack path in the "wavy-ring" pattern is geometrically described as

$$r = \frac{L}{2}\sin\left(\frac{2\pi}{\chi_\lambda}\psi\right) + R_0 - \frac{L}{2}, \tag{21}$$

where χ_λ is the dimensionless period, as shown in Figure 8(c). The relationship between the dimensionless width of the coffee ring χ_L and the dimensionless period of the "wavy-ring" pattern χ_λ is

$$\chi_\lambda \sim 2\chi_L, \tag{22}$$

which indicates that the width of the coffee ring determines the periodicity of the "wavy-ring" crack pattern.

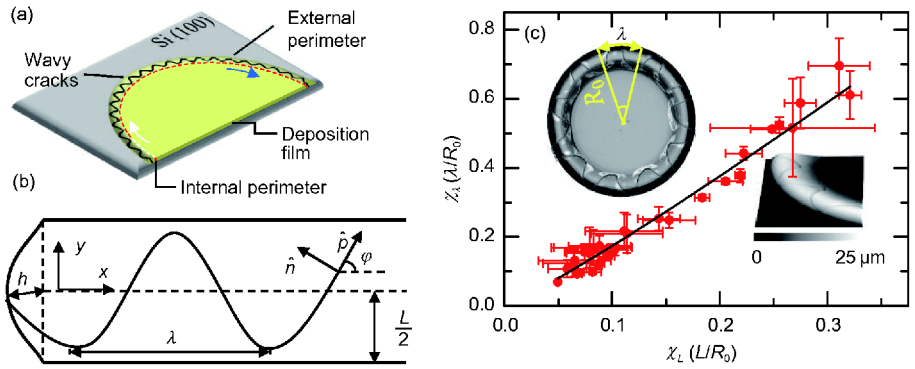

Figure 8 (Color online) The formation and periodicity of the "wavy-ring" pattern. (a) The outer and inner boundaries fixed the coffee ring to the substrate; (b) the crack path of "wavy-ring" crack pattern; (c) the dimensionless period is proportional to the dimensionless width of the coffee ring.

3.4 Relationship between the deposition film and the crack pattern

Certain parameters of the deposition patterns are used to quantify the conditions leading to each type of crack pattern. The dimensionless thickness χ_H is a function of the dimensionless width of the coffee ring χ_L, which fits our experimental data as the following scaling law:

$$\chi_L = 0.6\chi_H^{0.4}. \tag{23}$$

The above scaling law and the morphological diagram of crack patterns of drying protein droplets are shown in Figure 9. This graph is divided into four regions (Figure S1). In the first region ($\chi_H \sim 0$), drying droplets are deposited as typical coffee ring without any crack. Deposition film in this region is stable, since the thickness is too small to generate cracks. In the second region ($0 < \chi_H \leq 0.2$), the "wavy-ring" pattern forms in the coffee ring. In the third region ($0.2 < \chi_H \leq 0.55$), the "daisy" pattern shows up. The corresponding deposition film is also coffee ring. In this region, the minimum thickness of the central point exceeds a critical value, and numerous disordered cracks take shape in the center of the dried film. Meanwhile, spiral cracks are triggered in separated blocks. While in the last region ($\chi_H > 0.55$), to deposit a relatively uniform film, the concentration should be higher than 10%, which is that of the raw egg-white solution. Hence, the final crack pattern in the last region is not given.

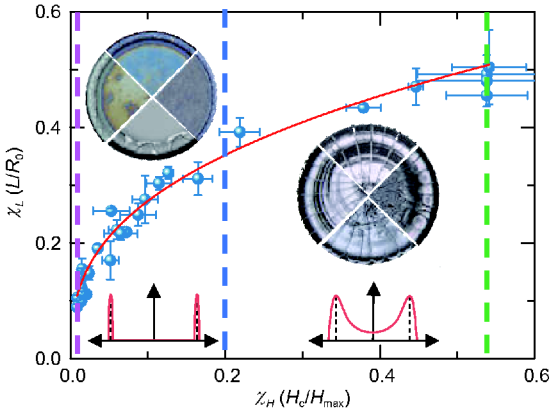

Figure 9 (Color online) Morphological diagram of crack patterns of drying protein droplets and the function of the dimensionless thickness and width. The dotted lines at $\chi_H \sim 0$, $\chi_H = 0.2$ and $\chi_H = 0.55$ divide the figure into four regions. In the first region, neither the central part nor the coffee ring generates crack. In the second region, wavy cracks in the coffee ring take the shape of "wavy-ring" pattern. The third region corresponds to the "daisy" crack pattern. The last region is related with a relatively flat film and a more concentrated protein solution is necessary.

4 Conclusions

Desiccation cracks and their patterns in drying droplets of protein solutions have been experimentally studied. We find that different dying processes cause different deposition and crack patterns. The experimental results reveal that the coffee-ring effect becomes more obvious as the concentration decreases. In addition, we identify two categories of crack patterns according to the position and shape of these arresting crack patterns, namely, "daisy" and "wavy-ring" patterns. We demonstrate that the "daisy" pattern appears in drying droplets with relatively high concentrations, whereas the "wavy-ring" pattern appears in drying droplets with low concentrations. Their formations and periodicities are explored. On one hand, the humidity gradient induces the radial crack propagation as the solvent evaporates. On the other hand, the coffee-ring effect tends to generate wavy cracks in the coffee ring. The relationship between the dimensionless width of the coffee ring and the dimensionless period of the "wavy-ring" pattern subjects to $\chi_\lambda \sim 2\chi_L$. The correlation between the deposition and the crack pattern is obtained. The deposition film is stable when the maximum thickness is too small to generate cracks. The "wavy-ring" crack pattern forms in the coffee ring as the thickness of the deposition

film increases. When the minimum thickness of the central part exceeds a critical value, the "daisy" pattern arises. This study will help in understanding the formation mechanisms of crack patterns in drying droplets of protein solutions and assisting the future design of crack patterns in practical applications.

This work was supported by the National Natural Science Foundation of China (Grant Nos. U1562105, 11372313), the Chinese Academy of Sciences through CAS Interdisciplinary Innovation Team Project, the Chinese Academy of Sciences Key Research Program of Frontier Sciences (Grant No. QYZDJ-SSW-JSC019), and the Chinese Academy of Sciences Strategic Priority Research Program (Grant No. XDB22040401).

Supporting Information

The supporting information is available online at tech.scichina.com and www.springerlink.com. The supporting materials are published as submitted, without typesetting or editing. The responsibility for scientific accuracy and content remains entirely with the authors. The supporting materials contain additional information about the experiments and results.

1 Kindle E M. Some factors affecting the development of mud-cracks. J Geol, 1917, 25: 135–144
2 Steward P A, Hearn J, Wilkinson M C. An overview of polymer latex film formation and properties. Adv Colloid Interf Sci, 2000, 86: 195–267
3 Wu D, Yin Y, Yang F, et al. Mechanism for controlling buckling wrinkles by curved cracks on hard-nano-film/soft-matter-substrate. Appl Surf Sci, 2014, 320: 207–212
4 Wu D, Xie H, Yin Y, et al. Micro-scale delaminating and buckling of thin film on soft substrate. J Micromech Microeng, 2013, 23: 035040
5 Sendova M, Willis K. Spiral and curved periodic crack patterns in sol-gel films. Appl Phys A-Mater, 2003, 76: 957–959
6 Dillard D A, Hinkley J A, Johnson W S, et al. Spiral tunneling cracks induced by environmental stress cracking in LaRC^{TM}-TPI adhesives. J Adhesion, 2006, 44: 51–67
7 Wan N, Xu J, Lin T, et al. Observation and model of highly ordered wavy cracks due to coupling of in-plane stress and interface debonding in silica thin films. Phys Rev B, 2009, 80: 014121
8 Liu T, Luo H, Ma J, et al. Tuning crack pattern by phase separation in the drying of binary colloid-polymer suspension. Phys Lett A, 2014, 378: 1191–1199
9 Marthelot J, Roman B, Bico J, et al. Self-replicating cracks: A collaborative fracture mode in thin films. Phys Rev Lett, 2014, 113: 085502
10 Boulogne F, Pauchard L, Giorgiutti-Dauphiné F. Annular cracks in thin films of nanoparticle suspensions drying on a fiber. Europhys Lett, 2013, 102: 39002
11 Ma H, Gao P, Fan D, et al. Radially aligned microchannels prepared from ordered arrays of cracks on colloidal films. Phys Chem Chem Phys, 2013, 15: 9808–9811
12 Kattouf B, Warwar C, Balla I, et al. Hexagonal patterns in thin films: Experiments and modeling. Extreme Mech Lett, 2015, 2: 65–71
13 Bucklow S. The description of craquelure patterns. Stud Conserv, 1997, 42: 129–140
14 Bucklow S. The description and classification of craquelure. Stud Conserv, 1999, 44: 233–244
15 Ball P. Watching paint dry. Nat Mater, 2004, 3: 851–851
16 Nakano A, Bachlechner M E, Branicio P, et al. Large-scale atomistic modeling of nanoelectronic structures. IEEE Trans Electron Devices, 2000, 47: 1804–1810
17 Zhao Y P. Nano and Mesoscopic Mechanics. Beijing: Science Press, 2014
18 Nam K H, Park I H, Ko S H. Patterning by controlled cracking. Nature, 2012, 485: 221–224
19 Fukuda K, Sekine T, Kumaki D, et al. Profile control of inkjet printed silver electrodes and their application to organic transistors. ACS Appl Mater Interfaces, 2013, 5: 3916–3920
20 Kim M, Ha D, Kim T. Cracking-assisted photolithography for mixed-scale patterning and nanofluidic applications. Nat Commun, 2015, 6: 6247
21 Zhao Y P. Physical Mechanics of Surfaces and Interfaces. Beijing: Science Press, 2012
22 Zhang Y, Qian Y, Liu Z, et al. Surface wrinkling and cracking dynamics in the drying of colloidal droplets. Eur Phys J E, 2014, 37: 84
23 Zhang Y J, Liu Z T, Zang D Y, et al. Pattern transition and sluggish cracking of colloidal droplet deposition with polymer additives. Sci China-Phys Mech Astron, 2013, 56: 1712–1718
24 Pauchard L, Parisse F, Allain C. Influence of salt content on crack patterns formed through colloidal suspension desiccation. Phys Rev E, 1999, 59: 3737–3740
25 Leung K T, Józsa L, Ravasz M, et al. Pattern formation: Spiral cracks without twisting. Nature, 2001, 410: 166–166
26 Néda Z, Leung K, Józsa L, et al. Spiral cracks in drying precipitates. Phys Rev Lett, 2002, 88: 095502
27 Wu D, Yin Y J, Xie H M, et al. Archimedes spiral cracks developed in a nanofilm/substrate system. Chin Phys Lett, 2013, 30: 036801
28 Pauchard L, Adda-Bedia M, Allain C, et al. Morphologies resulting from the directional propagation of fractures. Phys Rev E, 2003, 67: 027103
29 Dufresne E R, Stark D J, Greenblatt N A, et al. Dynamics of fracture in drying suspensions. Langmuir, 2006, 22: 7144–7147
30 Gauthier G, Lazarus V, Pauchard L. Alternating crack propagation during directional drying. Langmuir, 2007, 23: 4715–4718
31 Goehring L, Clegg W J, Routh A F. Solidification and ordering during directional drying of a colloidal dispersion. Langmuir, 2010, 26: 9269–9275
32 Mal D, Sinha S, Middya T R, et al. Desiccation crack patterns in drying laponite gel formed in an electrostatic field. Appl Clay Sci, 2008, 39: 106–111
33 Khatun T, Dutta T, Tarafdar S. Crack formation under an electric field in droplets of laponite gel: Memory effect and scaling relations. Langmuir, 2013, 29: 15535–15542
34 Pauchard L, Elias F, Boltenhagen P, et al. When a crack is oriented by a magnetic field. Phys Rev E, 2008, 77: 021402
35 Dugas V, Broutin J, Souteyrand E. Droplet evaporation study applied to DNA chip manufacturing. Langmuir, 2005, 21: 9130–9136
36 Brutin D, Sobac B, Loquet B, et al. Pattern formation in drying drops of blood. J Fluid Mech, 2011, 667: 85–95
37 Sobac B, Brutin D. Desiccation of a sessile drop of blood: Cracks, folds formation and delamination. Colloid Surface A, 2014, 448: 34–44
38 Pearce E. Spatial location studies on the chemical composition of human tear ferns. Ophthal Physl Opt, 2000, 20: 306–313
39 Annarelli C C, Fornazero J, Bert J, et al. Crack patterns in drying protein solution drops. Eur Phys J E, 2001, 5: 599–603
40 Golbraikh E, Rapis E G, Moiseev S S. On the crack pattern formation in a freely drying protein film. Tech Phys, 2003, 48: 1333–1337
41 Deegan R D, Bakajin O, Dupont T F, et al. Capillary flow as the cause of ring stains from dried liquid drops. Nature, 1997, 389: 827–829
42 Yu Y S, Xia X L, Zheng X, et al. Quasi-static motion of microparticles at the depinning contact line of an evaporating droplet on PDMS surface. Sci China-Phys Mech Astron, 2017, 60: 094612
43 Zhao Y P. Modern Continuum Mechanics. Beijing: Science Press, 2016
44 Sprakel J, Besseling N A M, Cohen Stuart M A, et al. Capillary adhesion in the limit of saturation: Thermodynamics, self-consistent field modeling and experiment. Langmuir, 2008, 24: 1308–1317
45 Bhardwaj R, Fang X, Somasundaran P, et al. Self-assembly of colloidal particles from evaporating droplets: Role of DLVO interactions

and proposition of a phase diagram. Langmuir, 2010, 26: 7833–7842
46 Hu H, Larson R G. Analysis of the microfluid flow in an evaporating sessile droplet. Langmuir, 2005, 21: 3963–3971
47 Hu H, Larson R G. Analysis of the effects of Marangoni stresses on the microflow in an evaporating sessile droplet. Langmuir, 2005, 21: 3972–3980
48 Sardan O, Yalcinkaya A D, Erdem Alaca B. Self-assembly-based batch fabrication of nickel-iron nanowires by electroplating. Nanotechnology, 2006, 17: 2227–2233
49 Bhardwaj R, Fang X, Attinger D. Pattern formation during the evaporation of a colloidal nanoliter drop: A numerical and experimental study. New J Phys, 2009, 11: 075020
50 Russel W B, Wu N, Man W. Generalized Hertzian model for the deformation and cracking of colloidal packings saturated with liquid. Langmuir, 2008, 24: 1721–1730
51 Goehring L, Nakahara A, Dutta T, et al. Desiccation Cracks and Their Patterns: Formation and Modelling in Science and Nature. Hoboken: John Wiley & Sons, 2015
52 Xia Z C, Hutchinson J W. Crack patterns in thin films. J Mech Phys Solids, 2000, 48: 1107–1131
53 Beuth Jr J L. Cracking of thin bonded films in residual tension. Int J Solids Struct, 1992, 29: 1657–1675
54 Griffith A A. The phenomena of rupture and flow in solids. Philos Trans R Soc A-Math Phys Eng Sci, 1921, 221: 163–198
55 Yin H M, Paulino G H, Buttlar W G. An explicit elastic solution for a brittle film with periodic cracks. Int J Fract, 2008, 153: 39–52
56 Allain C, Limat L. Regular patterns of cracks formed by directional drying of a collodial suspension. Phys Rev Lett, 1995, 74: 2981–2984
57 Lee W P, Routh A F. Why do drying films crack? Langmuir, 2004, 20: 9885–9888
58 Goehring L, Clegg W J, Routh A F. Wavy cracks in drying colloidal films. Soft Matter, 2011, 7: 7984–7987
59 Rice J R. Some remarks on elastic crack-tip stress fields. Int J Solids Struct, 1972, 8: 751–758
60 Fett T, Mattheck C, Munz D. On the calculation of crack opening displacement from the stress intensity factor. Eng Fract Mech, 1987, 27: 697–715